

1 **Service and Ultimate Behavior of Adjustable Bolted Steel Plate Connections**

2 Evan J. Gerbo, S.M.ASCE¹; Ashley P. Thrall, A.M.ASCE²; Theodore P. Zoli, P.E., M.ASCE³

3 **ABSTRACT**

4 This paper experimentally and numerically investigates the service and ultimate behavior of
5 adjustable bolted steel plate connections: slip-critical, splice plate connections that can join wide
6 flange sections at a range of angles as well as adjust in-situ to achieve additional angles or com-
7 pensate for erection and fabrication tolerances. The connection is comprised of plates that are cold
8 bent by press brake to a specific set of angles, forming a prefabricated, kit-of-parts. Adjustability
9 is achieved by further cold bending the plates in the field through bolt tightening. The slip and bolt
10 shear behavior of the connection was experimentally tested by applying an axial force on a wide
11 flange member (via a servo-controlled hydraulic actuator in displacement control) joined by the
12 tested connection to another wide flange member (restrained by a rigid reaction frame). A total of
13 18 scenarios were tested to investigate the effect of (1) direction and amount of cold bend via bolt
14 tightening, (2) tightening approaches, (3) direction of loading, and (4) plate and member angle on
15 behavior. A finite element numerical modeling approach was developed and validated, offering
16 additional understanding of bolt behavior in the adjustable bolted steel connection. A degradation
17 in slip capacity was observed due to a reduced clamping load. During bolt tightening, the bolts
18 deform non-flush plies into contact with the flanges and are simultaneously being bent by contact
19 with the plates, leading to this reduced clamping load. The bolt shear capacity can also be degraded
20 due to the connection geometry which can reduce the engagement of shear planes. Recommenda-
21 tions for reductions in slip and bolt shear capacity are developed. Importantly, findings also offer

¹PhD Candidate, Kinetic Structures Laboratory, Department of Civil & Environmental Engineering & Earth Sciences, University of Notre Dame, Notre Dame, IN 46556. E-mail: egerbo@nd.edu

²Myron and Rosemary Noble Associate Professor of Structural Engineering, Kinetic Structures Laboratory, Department of Civil & Environmental Engineering & Earth Sciences, University of Notre Dame, Notre Dame, IN 46556. (corresponding author) E-mail: athrall@nd.edu

³National Bridge Chief Engineer, HNTB Corp., Empire State Building, 350 5th Ave., 57th Floor, New York, NY 10118. E-mail: tzoli@hntb.com

22 insight into the behavior of bent connections, as well as misaligned or non-flush connections that
23 are force-fit in the field.

24 **Author Keywords:** Bolted steel connection; Slip-critical connection; Cold bending; Prefabrica-
25 tion; Rapid erection; Misaligned connection; Force-fitting

26 INTRODUCTION

27 Adjustable bolted steel plate connections [Figure 1, introduced in Gerbo et al. (2018) and
28 Gerbo et al. (2019a)] are a kit-of-parts approach to join angled structural members through cold
29 bending. Specifically, bent flange splice plates join flanges of wide flange sections in double
30 shear. It is envisioned that webs would also be joined in double shear using straight and flush
31 splice plates. The resulting slip-critical connection is moment-resisting as the webs and flanges
32 are joined independently. The bent flange plates are a prefabricated, kit-of-parts which are prebent
33 to prescribed angles ($\gamma = 5, 10, 15$ degrees, or a 0 degree non-bent plate) through cold bending
34 via a press brake (Figure 1A). To join members at a wider range of angles, α or to adjust for
35 erection and fabrication tolerances, the prebent flange plates can be further cold bent via bolt
36 tightening during installation (Figure 1C, D), i.e., bolts deform the non-flush plies (with difference
37 in ply angle $\delta = \alpha - \gamma$) to contact with the flange. In this way, the prefabricated, kit-of-parts
38 can be used for many connections within one structure or among different structures, leading to
39 construction cost and time savings through mass production of connection details. The adjustable
40 bolted steel plate connection is intended for connections between any two angled wide flange
41 members. Applications include both buildings (for example for the apex connections of portal
42 frames) and bridges (for example for angled connections in arches or trusses).

43 In prior research, the authors have (1) experimentally and numerically investigated the strains
44 induced in the plates due to prefabrication via press brake (Gerbo et al., 2016), and (2) experimen-
45 tally and numerically investigated the plate and bolt strains due to installation via bolt tightening
46 (Gerbo et al., 2018, 2019a,b). However, there is a major research gap in understanding the effect of
47 the installation process and the connection geometry on the service (or slip) and ultimate behavior
48 of these connections. During field installation, the bolts plastically deform the non-flush plates, are

49 in eccentric contact with the non-flush plates, and are bent by contact with the plates, all resulting
50 in degradation of the slip load. The peak bolt shear load can also be affected as the connection
51 geometry can result in shear planes not being fully engaged or not in contact.

52 This research has wider relevance in steel design, fabrication, and construction, specifically for
53 bent plates in skewed or kinked connections, as well as misaligned or non-flush connections. The
54 use of bent plate connections is commonplace in skewed and curved girder cross frame connections
55 for bridges and skewed beam connections in buildings. Bent plate connections between piecewise
56 straight components are also emerging as a cost-effective alternative to fabricating curved beams or
57 girders. Additionally, connections that are designed and fabricated as straight may be misaligned
58 in the field due to poor fit up. Force fitting of these connections can induce unanticipated forces
59 and/or distortion in these connections. How much misalignment and distortion can be tolerated,
60 and its effect on service and ultimate behavior is an important consideration in structural steel
61 design and detailing. Performance issues associated with plate contact, bolt hole geometry, bolt
62 flexure, and forces induced during bolt up are often issues with these types of connections. While
63 the behavior of slip-critical, straight and flush splice connections is well understood (Kulak et al.,
64 2001), the performance of bent and misaligned or non-flush connections has received compara-
65 tively little attention. The research presented in this paper is an important first step in developing
66 a comprehensive understanding of behavior of these bent and misaligned or non-flush and their
67 associated design implications.

68 This paper is the first investigation of the service and ultimate behavior of adjustable bolted
69 steel plate connections and the more general case of bent connections, as well as misaligned or
70 non-flush connections. The focus is on understanding slip behavior and the failure mode of bolt
71 shear.

72 **OBJECTIVES AND SCOPE**

73 The objective of this paper is to understand the service and ultimate behavior of adjustable
74 bolted steel plate connections. A total of 18 connection scenarios were experimentally tested to
75 failure under axial force at approximately 1/3 scale to understand the effect of (1) direction and

76 amount of cold bend via bolt tightening (Scenarios 3-5), (2) tightening approaches (Scenarios 6,7),
77 (3) direction of loading (Scenario 8), and (4) plate and member angle (Scenario 9-16) (Figure 2,
78 Table 1). Scenario 3 was a benchmark case that was tested 3 times to demonstrate repeatability.

79 The plates for each tested scenario were first prebent via press brake and then installed [fol-
80 lowing the installation procedures recommended by Gerbo et al. (2018) and Gerbo et al. (2019a)]
81 to join two wide flange members in a rigid reaction frame. A servo-controlled hydraulic actuator
82 in displacement control was then used to load the connection to failure via bolt shearing. As this
83 is the first investigation on the service and ultimate behavior of the adjustable bolted steel plate
84 connection, this study focused on the axial tension behavior of the connection, with the actuator
85 aligned concentrically with one of the joined wide flange members. The bolt shear failure mode
86 was investigated as the installation process induces bending in the bolts which can impact bolt per-
87 formance. Scenario 8, with a large gap between members, was tested in compression. However,
88 it is envisioned that the plates and gap between members would be appropriately dimensioned to
89 avoid the failure mode of plate buckling when loaded in compression. Throughout testing, the load,
90 actuator displacement, relative movement (or slip) of plates, plate surface strains, and residual bolt
91 surface strains were measured.

92 The measured data are compared to finite element (FE) numerical modeling, resulting in a
93 validated FE numerical modeling approach and providing further insight into bolt behavior. Rec-
94 ommendations for reductions in slip and bolt shear capacity are developed. Research results are
95 relevant to the behavior of bent connections, as well as misaligned or non-flush connections that are
96 force-fit in the field. Measured behavior of straight and flush control specimens provides further
97 insight into slip-critical connections in general.

98 **EXPERIMENTAL PROGRAM**

99 Tests were performed at approximately 1/3 scale, due to laboratory limitations. All compo-
100 nents, including the bolts, plates, and members, were scaled to ensure that the strain distributions
101 would be similar to full-scale connections. It is acknowledged that there are scaling effects related
102 to bolt size and clamping pressure. However, experiments would be able to capture the general

103 service and ultimate behavior of the connection. Each scenario used 4.76 mm (0.188 in.) thick
104 ASTM A36 steel plates joined the flanges of W4x13 wide flange members in double shear. Three
105 plates joined the top flanges (T) and three plates joined the bottom flanges (B). Single 88.9 mm
106 (3.50 in.) wide outer (O) plates and two 31.8 mm (1.25 in.) wide inner (I) plates straddled the web
107 connecting each flange. All plates were 152 mm (6.00 in.) long [except for Scenario 8 which are
108 212 mm (8.33 in.) long]. The plates were joined to each flange by 8, 6.35 mm (0.250 in.) diameter
109 SAE Grade 5 (SAE, 2014) bolts [equivalent mechanical properties and similar chemical properties
110 to ASTM A325 (ASTM, 2014a) bolts]. Two ASTM F436 (ASTM, 2018) washers were used with
111 each bolt, along with Grade A nuts. With the exception of Scenario 2 which used standard size
112 holes [7.14 mm (0.281 in.) diameter] in the plates and flanges, the flanges had long slots [7.14 mm
113 x 15.9 mm (9/32 in. x 5/8 in.)] and the plates had oversized holes [7.94 mm (5/16 in.)]. As the
114 connection was approximately 1/3 scale, the scaled oversized hole diameter was targeted to be 1/3
115 of the typical 3.18 mm (1/8 in.) larger than bolt diameter. This was rounded to the nearest available
116 drill bit size of 7.94 mm (5/16 in.). The long slots and oversized holes were selected to create a
117 versatile kit-of-parts with few number of unique components (Gerbo et al., 2018). Scenario 1 was
118 a straight and flush control specimen, with the same hole geometry as the adjustable bolted splice
119 plate connection (Figure 2A-C). Scenario 2 was also a straight and flush control specimen, but with
120 plates and flanges having standard size holes.

121 Prior to testing, the plates were prebent via press brake with a 38.1 mm (1.50 in.) radius to
122 angles, γ (Figure 1A). The radius is equivalent to $8t_s$, where t_s is the thickness of the plates. This
123 was selected as it exceeds the $5t_s$ minimum radius prescribed by recent revisions to bridge design
124 code (AASHTO, 2012).

125 The prebent plates were then installed via bolt tightening to join the two W4x13 members fol-
126 lowing the procedures recommended in Gerbo et al. (2018) and Gerbo et al. (2019a). The plates
127 and bolts were first loosely assembled on the W4x13 members, with assemblies adjusted to have
128 approximately the same starting position position. The nuts and washers were initially assembled
129 by hand, with the distance from the tip of the bolt to the face of the nut equalized among the bolts

130 to within 0.254 mm (0.01 in) to ensure a symmetric starting position. Bolt tightening was then
131 performed using a torque wrench. Tightening was performed in a criss-cross type pattern, pro-
132 gressing from bolt 1 through bolt 8 (Figure 1E-F), with 1 turn occurring per increment until firm
133 contact was achieved between plates and flanges at all bolt locations [firm contact was defined by
134 no longer being able to fit a 0.0762 mm (0.00300 in.) shim between the plates and flanges]. An
135 additional 5/6 turn of each bolt was then performed as an adaptation of the turn-of-nut criteria (Re-
136 search Council on Structural Connections, 2014). During installation, one W4x13 was supported
137 by a rigid reaction frame (with top and bottom flanges, as well as the web, bolted to the frame) and
138 the other was supported by a stub column (bottom flanges were bolted to the stub column, Figure
139 2A,D). The stub column was removed prior to testing the connection to failure.

140 Testing was then performed on the installed connection by applying an axial force on the
141 W4x13 member [moving member (M), hereafter], previously secured to the stub column, using a
142 servo-controlled hydraulic actuator [Parker 0.500 BB2HT14A 6.500, 20.7 MPa (3000 psi), 262 kN
143 (58.9 kips) capacity] in displacement control, at a rate of 0.457 mm/min. (0.0180 in./min.) (Figure
144 2B-C,E-F,G). The other W4x13 member [static member (S), hereafter] remained restrained to the
145 reaction frame. All tests were performed in tension, with the exception of Scenario 8 which was in
146 compression. Testing continued for each scenario until bolt failure or 50% drop in load (in the case
147 of Scenario 8). The self-reacting reaction frame was modular, with different positions for member
148 and hydraulic actuator to accommodate the tested scenarios. The focus of the research was on the
149 behavior of the flange plates and bolts. Therefore, no web splice plates were used.

150 Figure 2H-I shows the instrumentation. Displacements were measured using string poten-
151 tiometers (MD Totco 1850-002) and linear potentiometers (BEI 9615R5.1KL2.0). A linear poten-
152 tiometer (Balluff BTL6-A500-M0178-PF-S115) attached to the hydraulic actuator measured the
153 actuator displacement. Pressure transducers (Anfield TG-300P-G-3-M12-4MA3, 3000 psi) mea-
154 sured the force in the actuator. The TO and BO plate surface strains due to prebending via a press
155 brake, installation via bolt tightening, and loading to failure were measured using the photographic
156 measurement technique three-dimensional (3D) digital image correlation [DIC, see Gerbo et al.

157 (2016), Gerbo et al. (2018), and Gerbo et al. (2019a)]. An assembly of mirrors facilitated the DIC
158 measurements (Figure 2I). DIC was also used to measure the residual strains in the bolts.

159 The instrumentation confirmed that the self-reacting reaction frame had negligible deformation
160 during testing [less than 1.27 mm (0.05 in.)]. The static member elastically displaced relative to the
161 reaction frame, as measured by the string potentiometers. In the actuator force, F versus actuator
162 displacement, Δ plots, this elastic displacement was removed by projection along the actuator axis.

163 MATERIAL PROPERTIES

164 Table 2 provides the measured material properties of the ASTM A36 (ASTM, 2014b) plates
165 and the SAE Grade 5 (SAE, 2014) bolts used in the experimental tests. ASTM material testing of
166 the plates was performed using an Instron 5590 Universal Testing Machine (ASTM, 2017b,a,c,d).
167 A total of 5, full thickness [4.76 mm (0.188 in.)] samples (all from the same bar) were tested, ac-
168 cording to the required ASTM dimensions (ASTM, 2017a) for a 50.8 mm (2 in.) gauge length. The
169 tensile testing was performed in the same direction as the final direction of rolling of the samples
170 (ASTM, 2017b). This corresponds to the longitudinal axis of the connection (Figure 1). ASTM
171 material testing of 5 bolts was performed by Laboratory Testing, Inc. (Hatfield, Pennsylvania)
172 according to ASTM standards (ASTM, 2016).

173 NUMERICAL MODELING

174 3D FE numerical analyses of the connection behavior were performed in ABAQUS Standard
175 (ABAQUS, 2014), using C3D8R solid elements with a typical mesh size of 1.02 mm (0.04 in.) in
176 the plates, 0.508 mm (0.02 in.) in the bolts, and 2.54 mm (0.1 in.) in the wide flange members.
177 Nonlinear material models with isotropic hardening were used for the plate and bolts, based on the
178 measured stress-strain behavior (Table 2). Geometric nonlinearity was also used.

179 Symmetry about the longitudinal direction was employed to reduce computational expense
180 (Figure 3). Boundary conditions to enforce symmetry included translation restraints in the x-
181 direction along the longitudinal centerline of the connection. Boundary conditions to simulate the
182 self-reacting frame included translation restraints in all 3 directions along the truncated face of the

183 static member. During bolt installation, the truncated face of the moving member has the same
184 restraints. The bolt tightening process was simulated using the approach developed and validated
185 in Gerbo et al. (2019a). After bolt installation, the restraints on the truncated face of the moving
186 member were removed, allowing the connection to elastically spring back (simulating removal of
187 the stub column). The actuator was simulated using a slot-type connector to induce displacements
188 while allowing in plane rotation at each end of the actuator.

189 To include the effect of residual strains and strain hardening from prefabrication via press
190 brake, the bending process was first modeled using the approach developed and validated in Gerbo
191 et al. (2016).

192 **BEHAVIOR OF STRAIGHT AND FLUSH BOLTED SPLICE CONNECTIONS**

193 Figure 4 shows the actuator force, F versus actuator displacement, Δ for the two straight and
194 flush scenarios, with slip and peak load provided in Table 1. Scenario 1 had a 15.5% higher
195 measured load at slip initiation compared to Scenario 2. This can be attributed to “caving” of
196 the plates into the long slots in the flanges, increasing frictional resistance. The initiation of slip
197 and its location is identified by a marker. As expected, the slip plateau of Scenario 1 was much
198 longer than Scenario 2 due to the additional play provided by the long slots. Both Scenario 1 and
199 2 reached similar peak loads, with Scenario 1 being just 3.36% higher, demonstrating that the hole
200 size did not impact peak load.

201 **Closed-Form Design Code Predictions**

202 Current design code (AISC, 2017) predicts slip capacity, ϕR_{n-Slip} for straight splice connec-
203 tions as:

$$\phi R_{n-Slip} = \phi \mu D_u h_f T_b n_s n_b \quad (1)$$

204 where ϕ is a factor considering hole size [1 for standard holes, 0.7 for long slots (in this paper,
205 comparisons use the 0.7 value for consistency, even though Scenario 2 should use 1.0), μ is the
206 mean slip coefficient (0.30 for Class A surfaces), D_u is a multiplier reflecting the ratio of mean
207 installed bolt pretension to the specified minimum bolt pretension (1.13), h_f is a factor for fillers

208 (1.0 for no fillers), T_b is the minimum fastener tension force, n_s is the number of slip or shear
 209 planes per bolt (2), and n_b is the number of bolts (4). T_b is typically provided in design code
 210 (AISC, 2017), but the size of the bolts in this research were smaller than those provided in the
 211 code. Instead, T_b is calculated per the recommendation of AISC (2017) as:

$$T_b = 0.70F_t A_s \quad (2)$$

212 where F_t is the minimum specified tensile strength [830 MPa (120 ksi), (SAE, 2014)], and A_s is
 213 the stress area in metric units (ASTM, 2015):

$$A_s = 0.7854[D - (0.9382P)]^2 \quad (3)$$

214 where D is the bolt diameter [6.35 mm (0.250 in.)] and P is the thread pitch [1.27 mm (0.05 in.)].
 215 Therefore, $\phi R_{n-Slip} = 23.0$ kN (5.16 kips) for long slots and $\phi R_{n-Slip} = 32.8$ kN (7.37 kips) for
 216 standard holes.

217 Using these predictive equations, Scenario 2 should actually have a higher slip load than Sce-
 218 nario 1. The measured slip load of Scenario 2 does not even achieve the design code prediction.
 219 This sample size is too small to make recommendations related to this difference, but it indicates
 220 an area for future research. The measured slip load for Scenario 1 exceeded the predicted slip load
 221 (using $\phi=0.7$).

222 The predicted bolt shear capacity, $\phi R_{n-Shear}$ from current design code (AISC, 2017) is:

$$\phi R_{n-Shear} = \phi F_{nv} A_b n_s n_b \quad (4)$$

223 where ϕ is a reduction factor (0.75), F_{nv} is the nominal shear stress of the bolt [469 MPa (68
 224 ksi), (AISC, 2017)], and A_b is the nominal area of the bolt [31.7 mm² (0.0491 in.²)]. Both single
 225 (subscript 1) and double shear (subscript 2) are compared in this paper with $\phi R_{n-Shear-1} = 44.6$
 226 kN (10.1 kips) and $\phi R_{n-Shear-2} = 89.2$ kN (20.1 kips). Scenario 1 and 2 both exceed this design

227 code prediction.

228 **BEHAVIOR OF ADJUSTABLE BOLTED STEEL PLATE CONNECTION**

229 Figure 4 also compares the measured force-displacement behavior of the benchmark adjustable
230 bolted steel plate connection (Scenario 3) with the two straight and flush control specimens.

231 The benchmark Scenario 3 was tested three times to demonstrate repeatability. Among the
232 three tests, the measured slip load varied up to 21.5% compared to the average measured value of
233 12.4 kN (2.79 kips). The measured peak load varied just 4.98% compared to the average measured
234 value of 90.3 kN (20.3 kips). The higher variability of the slip load can be attributed to differences
235 in surface roughness. All three tests had slip initiate at a bottom flange faying surface, with the
236 final slip occurring at a top flange faying surface. The length of the measured slip plateau and
237 the displacement at peak load were similar among the three tested scenarios [varying up to 4.80%
238 compared to the average of 12.7 mm (0.500 in.)].

239 **Comparison to Straight and Flush Connections and Closed-Form Design Code Predictions**

240 Scenario 3 tests had an average reduction in measured slip load of 57.3% compared to Scenario
241 1. While Scenario 1 exceeded the predicted slip load, ϕR_{n-Slip} (with $\phi = 0.7$) by 26.4%, the
242 average measured slip load for Scenario 3 was 46.1% below ϕR_{n-Slip} . These tests also had a
243 reduced measured peak load, averaging 41.3% less than Scenario 1 and just 1.42% more than the
244 predicted double shear capacity, $\phi R_{n-Shear-2}$.

245 **Mechanics Based Understanding of Behavior**

246 Compared to a straight and flush scenario, the bolts of adjustable bolted steel plate connections:
247 (1) need to deform non-flush plates to contact with flanges (overcoming the difference in ply angle,
248 δ), hereafter δ -effect (Figure 5A) and (2) are bent by contact with the plates (oversized plate holes
249 and long slots in the flanges enable a bolt to fit through all three plies prior to bolt tightening,
250 but the bolt will be deformed flexurally through plate contact during tightening, Figure 5B-C),
251 hereafter interference-effect. In the δ -effect, the additional force needed to bring non-flush plies
252 together reduces clamping load of the bolts (Figure 5A). Further, as the bolts are in eccentric

253 contact with the initially non-flush plies, flexure also occurs, further degrading the clamping load.
 254 These mechanisms degrade the clamping load, reducing the slip capacity of the connection. This
 255 δ -effect only occurs in scenarios for non-zero δ . In the interference-effect, bending in the bolts
 256 causes plate contact during bolt installation resulting in friction between the bolt shank and edge
 257 of the plate holes (F_n in Figure 5B), reducing the clamping load along the bolt axis. The catenary
 258 action in the bolt redirecting the bolt pretension around the corner of the plate hole edge results in
 259 further frictional losses (F_c in Figure 5C). These mechanisms also degrade clamping load, reducing
 260 the slip capacity. This interference-effect only occurs when the bolts contact the plates during
 261 installation. The δ -effect and the interference-effect induce flexure in the bolts, contributing also
 262 to a reduction in bolt shear capacity. Both of these effects could occur for the more general case of
 263 bent connections, as well as non-flush (related to the δ -effect) or misaligned (where holes are not
 264 aligned, related to the interference-effect) connections. Force fitting is typically performed on non-
 265 flush or misaligned connections, but reductions in capacity from force fitting are not considered in
 266 design.

267 An analytical indicator of the interference-effect is the metric e_b [Figure 5C, first developed in
 268 Gerbo et al. (2019a)] which is an approximation of the amount of bolt deformation due to plate
 269 contact occurring during installation. This e_b metric is calculated as:

$$e_b = e_h - (d_{ph} - d_b) \quad (5)$$

270 where e_h is the offset between the plate holes (Figure 5D), calculated as:

$$e_h = |(t_m + t_s) \tan \alpha| + \frac{e_d}{\cos \alpha} \quad (6)$$

271 where t_m is the thickness of the flange, t_s is the thickness of the plates, d_{ph} is the plate hole

272 diameter, d_b is the diameter of the bolt, and e_d is determined as follows:

$$e_d = \begin{cases} l_{\delta 1}(\cos \gamma - \cos \alpha) & \text{if } \delta \geq 0 \\ g(\cos \gamma - \cos \alpha) & \text{if } \delta < 0 \end{cases} \quad (7)$$

273 where $l_{\delta 1}$ is the distance from flange edge to the center of its hole and g is the gap between
274 wide flange members (Figure 1C). Note that negative or zero values of e_b indicate that there is
275 no interference-effect.

276 The reduced measured slip load of Scenario 3, with $\delta = 2.5^\circ$ and one of the highest value
277 of e_b in the experimental testing program (Table 1), can be attributed to both the δ -effect and the
278 interference effect.

279 The adjustable bolted steel plate connection is intended to be in double shear for economy in
280 number of fasteners. However, depending on the offset between the plate holes, e_h only the shear
281 plane towards the convex side of the connection may be fully engaged, with the other partially
282 engaged or not at all (Figure 5D). This is due to the holes in the plates having identical locations in
283 the prebent state. This partial engagement of one of the shear planes was evident in the deformed
284 shape, measured via DIC, of an example bolt from Scenario 3a compared to one from Scenario
285 1 in which both shear planes are engaged (Figure 6A). Figure 6B shows the location of the bolt
286 centerline (based on measured DIC data) for all bolts in Scenario 1 and 3a. As the bolt centerline
287 crosses the shear planes, full shear engagement would be indicated by a vertical jump in the cen-
288 terline. Figure 6B shows that occurs for all shear planes of Scenario 1, indicating full double shear
289 behavior. Scenario 3a shows engagement at a single shear plane, indicating single shear behavior.

290 **Effect of Direction and Amount of Cold Bend via Bolt Tightening**

291 To investigate the effect of direction ($\pm \delta$) and amount ($|\delta| = 0^\circ$ or 2.5°) of cold bending via
292 bolt tightening while maintaining a constant member angle $\alpha = 12.5^\circ$, Scenario 5 ($\delta = -2.5^\circ$) is
293 compared with Scenario 3 ($\delta = 2.5^\circ$) and a flush Scenario 4 ($\delta = 0^\circ$) in Figure 4.

294 Notably, the flush and $-\delta$ scenarios had similar slip loads [15.9 kN (3.57 kips) and 16.6 kN
295 (3.74 kips), respectively], which were 45.9% and 48.1% higher than the average of the bench-

296 mark Scenario 3 tests. While the slip loads for flush and $-\delta$ scenarios are higher than benchmark
297 Scenario 3, they are 45.2% and 42.6% lower, respectively than Scenario 1.

298 The higher slip load for the flush scenario can be attributed to the lack of δ -effect and a reduced
299 interference-effect as Scenario 4 has a lower value of e_b . In the $-\delta$ scenario, there was a δ -effect,
300 but it was reduced as the plates were being bent in the opposite direction compared to prefabrication
301 via press brake. As a result of the Bauschinger effect, their yield strength in the direction of field
302 bending via bolt tightening would be reduced, thereby reducing the amount of force required to
303 bring the plies into contact. The interference-effect was also reduced due to a lower e_b .

304 The direction and amount of δ also impacted the progression of slip. Figure 7 shows the slip
305 of each faying surface as a function of actuator displacement, Δ . The measurements at inner pairs
306 of plates generally agree with each other, and were therefore averaged for simplicity. Straight
307 and flush Scenario 1 showed that the plies of the top flanges and bottom flanges slipped nearly
308 simultaneously, as expected. In contrast, all plies of the bottom flange of Scenario 3a slipped
309 prior to the plies of the top flange. The flush Scenario 4 showed similar behavior to Scenario 3a,
310 with the bottom flanges slipping before the top flanges. This was because there was still a slight
311 preference to slip the bottom flange first due to the bent portion of the plate contacting the edges of
312 the member flanges. The $-\delta$ Scenario 5 had near simultaneous slip of the top and bottom flanges.
313 This was due to the elastic strains induced in the plates during installation via bolt tightening and
314 the location of plate contact. Specifically, the elastic strains from installation spring the connection
315 back towards the initial plate angle. In $+\delta$ scenarios this results in the top flange being preloaded
316 in compression, and the bottom flange being preloaded in tension. When tensile loads were then
317 applied, the bottom flange slipped first. The contact location between plates and the flange resulted
318 in additional stored elastic energy for a similar springback effect. The springback effect from $-\delta$,
319 though it would be in the opposite direction, would be less in magnitude due to the Bauschinger
320 effect. This scenario also did not have the same plate contact location which causes the preference
321 toward bottom flange slip.

322 The direction and amount of cold bending via bolt tightening did not substantially influence the

323 peak loads. All 3 scenarios, which have similar e_h values, do not achieve shear capacities similar
324 to Scenario 1, indicating that only one shear plane was being fully engaged.

325 **Effect of Varying Tightening Approaches**

326 Two alternative bolt tightening approaches were investigated: (1) Scenario 6 using beveled
327 washers and (2) Scenario 7 where additional tightening was applied to each bolt.

328 As there was an observed reduction in slip and peak load in the adjustable bolted steel plate
329 connection, Scenario 6 investigated the use of beveled washers to reduce the effect of eccentric
330 contact at the bolt head and nut due to the difference in ply angle δ . The angle of the bevel was
331 2.5° , matching the magnitude of δ . Scenario 6 had a 49.1% lower slip load and a 12.9% lower peak
332 load than the comparable Scenario 3. Beveled washers create directionality to the bolt pretension
333 which precipitates slip in a particular direction at low loads. The reduction in ultimate load was
334 a result of the bolts being angled relative to the plates (as opposed to perpendicular to the plates)
335 in the final tightened position. This places the bolts even more into a single shear environment as
336 opposed to double shear. Beveled washers are therefore not recommended. Indeed, the bottom
337 plies of the static member actually slipped during the removal of the stub column.

338 In Scenario 7, the tightening procedure was altered to consider firm contact when not only
339 the plates have contacted the flange, but also the bolt head and nut were in firm contact with the
340 washers. This resulted in an extra 1/2 turn. This increased tightening was investigated as a potential
341 means of compensating for the observed loss in slip capacity. Bolt 6 on the bottom flange of the
342 static member broke during installation, indicating that too much bolt pretension was applied.
343 While 5 of the bolts were able to be tightened to this amount, the torque required to tighten the
344 nuts started to decrease towards the end of tightening, indicating that the bolts were close to failure.
345 This increased bolt tightening is not recommended.

346 **Effect of Direction of Loading**

347 Scenario 8 was tested in compression. A larger gap, g between the members [63.5 mm (2.50
348 in.)] was used as the gap for all other scenarios [4.24 mm (0.167 in.)] would have resulted in
349 bearing of the members after partial slip. Figure 8 shows the force-displacement curve for Scenario

350 8 compared to Scenario 3a, both with the same member and plate angles. The slip load for Scenario
351 8 was just 1.6% higher than the average of Scenarios 3a, 3b, and 3c, indicating no change to the slip
352 load. Scenario 8 had slip initiate at the top flange first as opposed to the bottom flange in Scenario 3.
353 This was because of the internal stresses developed during the installation process, which attempt to
354 spring the connection back towards the initial plate angles, as discussed earlier. For $+\delta$ scenarios,
355 the elastic springback preloads the top flange in compression, causing it to slip before the bottom
356 flange when loaded in compression. The peak load in Scenario 8 was significantly reduced. This
357 was expected as an angled or bent connection (i.e., member angle, α) was placed in compression
358 as opposed to tension. Failure was defined as 50% drop in load. No bolts were broken.

359 **Effect of Varying Plate and Member Angles**

360 The kit-of-parts for the adjustable bolted steel plate connections is comprised of plates with
361 initial angles $\gamma = 0, 5, 10, 15^\circ$. These connection plates were tested at varying member angles,
362 α with varying differences in initial ply angle, δ . Figure 9 shows the force-displacement curves
363 corresponding to each of these scenarios, demonstrating experimental evidence of behavior.

364 The slip and ultimate behavior of this kit-of-parts are compared with the behavior of the other
365 tested scenarios in Figure 10 and Figure 11, respectively. The measured force F (with subscript
366 s for slip force and p for peak force) is normalized with respect to the closed-form design predic-
367 tions, where a value above 1 indicates conservatism and below 1 indicates unconservatism. The
368 horizontal axis indicates the metrics e_b and e_h , normalized with respect to the bolt diameter d_b . The
369 markers correspond to the scenario number.

370 Figure 10 shows the impact of the δ -effect and the interference-effect (measured by e_b , with
371 negative e_b indicating no interference) on the measured slip load. Flush Scenario 10, as well as
372 the straight and flush control Scenario 1 and 2, have no δ - or interference-effects and have compa-
373 rable slip loads. Scenario 9 and 12, for which there was only the δ -effect, show slightly reduced
374 slip loads, but all are still conservative with respect to the design code predictions. In contrast,
375 Scenarios 13, 4, and 15 only have the interference-effect. Scenarios 13, 4 and 15 show significant
376 degradation of slip load and demonstrate that the design code predictions are unconservative when

377 bolts are bent by plate contact during installation. Comparing the impact of the δ -effect to the
378 interference-effect, the interference-effect dominates behavior. For scenarios with both the δ - and
379 interference-effects, there is a trend of decreasing measured slip load with increasing e_b/d_b

380 Figure 11 investigates the peak load of the scenarios, compared with the analytical approxi-
381 mation for the offset between the plate holes, e_h . e_h/d_b is compared with the required minimum
382 elongation for the relevant bolt standard [in this case 14%, (SAE, 2014)]. If e_h/d_b is less than the
383 minimum elongation strain, this ensures that the bolt can sufficiently deform, without rupture, to
384 engage the lagging shear plane. The measured amount of shear plane deformation, s is investi-
385 gated in Figure 12. s is calculated by taking the difference in the measured lateral location of the
386 centerline of the deformed bolt across a shear plane and normalizing by the bolt diameter (e.g.,
387 Figure 6B). A zero value indicates no shear. Larger values indicate increased shear deformation,
388 with a peak possible value 0.237 based on the measured rupture strains from tensile testing.

389 Scenarios 1, 2, 9, and 12 all have large values of s at both shear planes, indicating full shear
390 engagement. The measured peak load of these scenarios in Figure 11 also indicates double shear
391 behavior. This confirms that the limit that e_h/d_b be less than the minimum elongation strain ensures
392 double shear behavior. Indeed, Scenarios 1, 2, 9, and 12 all have peak loads far exceeding the
393 design code prediction for double shear.

394 For scenarios with e_h/d_b greater than the required elongation, both shear planes are not fully
395 engaged. Figure 12 shows that with increasing e_h/d_b , s decreases for the shear plane near the head
396 (for the top flange bolts) or the shear plane near the tip (for the bottom flange bolts), indicating
397 lack of engagement. For these cases with e_h/d_b greater than the required elongation, the measured
398 peak load was reduced. A designer could conservatively design these scenarios assuming single
399 shear behavior.

400 Data is not shown for Scenario 16 as a bolt broke during installation. e_b/d_b values should be
401 kept below 0.5, as this was found to rupture bolts in Scenario 16.

402 Numerical Predictions

403 The FE numerical model for Scenario 3 predicted a slip load of 14.0 kN (3.14 kips), 12.9%
404 higher than the average measured slip load from the Scenario 3 tests (Figure 10). The predicted
405 peak load was 98.3 kN (22.1 kips), just 8.66% higher than the average measured value (Figure 11).
406 In comparison, the FE numerical model for straight and flush Scenario 1 predicted a slip load of
407 52.5 kN (11.8 kips), 81.0% higher than the measured slip load and a peak load of 173 kN (39.0
408 kips), 12.3% higher than than the measured peak load.

409 Generally, the FE models were able to more closely predict the peak load compared to the
410 slip load for both Scenario 1 and Scenario 3. The slip load prediction is highly dependent on
411 the frictional coefficient between the plies and the amount of applied clamping load. In the FE
412 models, a frictional coefficient of 0.33 was assumed as recommended for steel-on-steel faying
413 surfaces (Kulak et al., 2001; AASHTO, 2014). In reality, the frictional coefficient may have been
414 different and may have varied among the faying surfaces. In the FE models, the applied clamping
415 load via bolt tightening was simulated by an induced displacement. This does not capture the
416 combined stress state of torsion and tension while tightening the bolt. Indeed, it was observed that
417 the bolt tips rotated 25 degrees, on average for all scenarios, relative to the head during tightening.
418 This difference may have impacted the clamping load. Differences in the prediction of the peak
419 load can be attributed also to this approach to simulating bolt tightening, as well as the assumed
420 isotropic material properties for the bolt based on tensile tests. Construction imperfections of the
421 experimental test setup may have also impacted both the slip and peak loads. The measured slip
422 load of Scenario 1 may have been especially impacted by any construction imperfections as such
423 imperfections may have imparted moment in a scenario for which only axial load was considered
424 in the FE model.

425 The FE models predicted a higher stiffness than the measured data, particularly for small dis-
426 placements prior to slip. This difference can be attributed to play in the connection of the actuator
427 to the moving member. The FE models for both Scenario 1 and Scenario 3 were able to accurately
428 predict the deformed residual shape of the bolts (Figure 6A), with FE model for Scenario 1 pre-

429 dicting a double shear environment and the FE model for Scenario 3 predicting more of a single
 430 shear environment.

431 The FE models were able to show the loss in bolt tension, B due to the δ - and interference-
 432 effects in Scenario 3 compared to Scenario 1 (Figure 13). While Scenario 1 shows a constant bolt
 433 tension along the length of the bolt, Scenario 3 indicates losses in bolt force toward the head of the
 434 bolt due to the mechanisms shown in Figure 5. Likewise, bending, M in the bolt is also shown for
 435 Scenario 3 in Figure 13, while no bending is shown for Scenario 1.

436 Analytical Predictions for Slip Load

437 Analytical predictions to capture the degradation in slip load were developed, incorporating the
 438 δ - and interference-effects. Specifically, a method to predict the bolt tension, T'_b was developed,
 439 where:

$$T'_b = T_b - F_\delta - F_h - F_c \quad (8)$$

440 where T_b is the bolt force for a straight and flush connection as given by design codes. The δ -effect
 441 is considered by reducing the bolt force by a prediction, F_δ of the force to plastically deform the
 442 plies into firm contact (Figure 5A). The flexural strains in the bolts from the δ -effect are ignored.
 443 The interference-effect is considered by accounting for the force, F_h from the friction between
 444 the plates and bolts due to bolt bending during installation (Figure 5B) and the force, F_c from the
 445 friction from the catenary action of the bolt redirecting the bolt pretension around the corner of the
 446 plate hole edge (Figure 5C).

447 An analytical approximation for F_δ considers the force required to deform the plates, assuming
 448 that a full plastic hinge forms in TO at flange contact or the net section of TI: $F_\delta = \max(M_{ppf}/l_{\delta 1},$
 449 $M_{ppn}/l_{\delta 2})$, where M_{ppf} is the plastic moment capacity of the gross cross section of the plate ($F_u Z_x$,
 450 where F_u is the ultimate stress and Z_x is the plastic section modulus of the plate), M_{ppn} is the
 451 plastic moment capacity of net section of the plate, and $l_{\delta 1}$ and $l_{\delta 2}$ are defined in Figure 5A. This
 452 assumption is conservative as not all δ would result in a full plastic hinge forming.

453 The frictional force, F_h is calculated as: $F_h = \frac{2M_{pb}\mu}{t_m}$, where M_{pb} is the plastic moment capacity

454 of the bolt ($F_{ub}Z_{xb}$, where F_{ub} is the ultimate stress and Z_{xb} is the plastic section modulus of the
455 bolt) and μ is the coefficient of friction. This assumes that plastic hinges form at the locations
456 shown in Figure 5B.

457 The loss from catenary action, F_c is approximated as follows: $F_c = T_b\mu \sin \Theta$, where Θ is the
458 angle over which the bolt must deform to accommodate the mis-aligned holes. Θ is calculated as:
459 $\Theta = \tan^{-1}\left(\frac{e_b}{t_m}\right)$

460 The predictions from this method are included as markers on Figure 10. Predictions are con-
461 servative and follow the same general trends as the measured data. For scenarios with low, but
462 positive e_b , they become overly conservative due to the assumptions of fully plastic bolt and plate
463 behavior. However this is a minor limitation to this predictive method.

464 These analytical predictions can also be compared to the FE predictions for tension in the bolt
465 (Figure 13). Specifically, in the middle of the bolt, the FE model predicted a bolt tensile force
466 of 19.0 kN (4.27 kips) for Scenario 1 and 14.3 kN (3.21 kips) for Scenario 3. The analytical
467 predictions T'_b are 12.1 kN (2.72 kips) for Scenario 1 (i.e., no reduction) and 4.04 kN (0.908 kips)
468 for Scenario 3. This further indicates that the analytical predictions are conservative compared to
469 the FE predictions. This conservatism can be attributed to the assumption of fully plastic bolt and
470 plate behavior in the analytical predictions.

471 CONCLUSIONS

472 This paper presented an experimental and numerical investigation of the behavior of adjustable
473 bolted steel plate connections under axial load. The focus was on understanding the effect of the
474 installation process and the connection geometry on the slip behavior and bolt shear failure mode of
475 these connections. Based on these experimental and numerical studies, the following conclusions
476 are made. Note that these conclusions may only be relevant to the specific scenarios studied in this
477 research including ASTM A325 bolts (SAE Grade 5 equivalent), shallow member angles up to α
478 = 17.5° , difference in ply angle, δ up to 2.5° , oversized plate holes, and long slot flange holes.

- 479 • Measured slip loads for the adjustable bolted steel plate connections were found to be lower

480 than a comparable straight ($\alpha = 0^\circ$) and flush ($\delta = 0^\circ$) control scenario. This is due to the
481 bolt installation process where bolts deform non-flush plates to contact with flanges and are
482 being bent by contact with the plates. Both mechanisms degrade the clamping load.

- 483 ● The measured slip load for scenarios where there is significant bolt deformation during
484 installation ($e_b/d_b > 0$) during field installation is below the predicted design slip capacity.
485 A mechanics-based method for predicting the slip load using geometric parameters has
486 been developed.
- 487 ● Measured peak loads for the adjustable bolted steel plate connection, for a failure mode
488 of bolt shear, are found to be lower than a comparable straight and flush control scenario.
489 While the connection is intended to be in double shear, the geometry of the connection
490 (e_h/d_b greater than the minimum required elongation strain of the bolt) can result in only
491 one shear plane being fully engaged, with partial or no engagement of the other.
- 492 ● As the expected shear capacity was reduced, a design engineer should consider single shear
493 capacity when e_h/d_b is greater than the minimum required elongation strain of the bolt from
494 the applicable material specification, as well as a resistance factor.
- 495 ● Bolt deformation, as classified by e_b/d_b and e_h/d_b ratios, has an impact on slip and bolt
496 shear capacity, respectively, as defined above. A geometric limit ($e_b/d_b < 0.5$) on the
497 amount of permissible bolt deformation during bolt tightening has been developed to pre-
498 vent bolt rupture during installation. High e_b/d_b values up to 0.3 were found to be accept-
499 able with capacity reductions for slip and bolt shear due to the large strain to failure for the
500 bolts in this research (measured elongation of 0.237).
- 501 ● The ultimate capacity of the connection in compression is significantly lower than the con-
502 nections in tension, as expected. The slip load was similar to that in tension.

503 Importantly, this research demonstrates that the slip and ultimate behavior of bent plate con-
504 nections (common in skewed and curved girder cross frame connections for bridges and skewed
505 beam connections in buildings) and misaligned and/or non-flush connections which are force-fit in
506 the field may be degraded and not adequately represented in current design guidance. This is an

507 area for future research.

508 **DATA AVAILABILITY STATEMENT**

509 Some or all data, models, or code generated or used during the study are available from the
510 corresponding author by request

511 **ACKNOWLEDGMENTS**

512 This material was based upon work supported by the National Science Foundation under Grant
513 No. CMMI-1351272. The support of Program Managers Drs. Kishor Mehta, Y. Grace Hsuan,
514 and Joy Pauschke is gratefully acknowledged. This research was also supported by the O. H.
515 Ammann Research Fellowship which was awarded to author Evan Gerbo. The authors are grateful
516 to Infra-metals and Steel Dynamics, Inc. for material donation and support.

517 **REFERENCES**

518 AASHTO (2012). *AASHTO LRFD Bridge Construction Specifications*. American Association of
519 State Highway and Transportation Officials (AASHTO), 2012 Interim Revisions to 3rd Edition,
520 Washington, D.C.

521 AASHTO (2014). *AASHTO LRFD Bridge Design Specifications, Customary U.S. Units*. American
522 Association of State Highway and Transportation Officials (AASHTO), 7th Edition, with 2015
523 and 2016 Interim Revisions, Washington, D.C.

524 ABAQUS (2014). “ABAQUS/Standard Analysis User’s Manual Version 6.14. Dassault Systemes,
525 Waltham, MA.

526 AISC (2017). *Steel Construction Manual*. American Institute of Steel Construction (AISC),
527 Chicago, IL, 15th edition.

528 ASTM (2014a). “ASTM A325-14: Standard specification for structural bolts, steel, heat treated,
529 120/105 ksi minimum tensile strength.” ASTM International. West Conshohocken, PA.

530 ASTM (2014b). “ASTM A36/A36M-14: Standard specification for carbon structural steel.”
531 ASTM International. West Conshohocken, PA.

532 ASTM (2015). “ASTM F3125/F3125M-15a: Standard specification for high strength structural
533 bolts, steel and alloy steel, heat treated, 120 ksi (830 mpa) and 150 ksi (1040 mpa) minimum
534 tensile strength, inch and metric dimensions.” ASTM International. West Conshohocken, PA.

535 ASTM (2016). “ASTM F606/606M-16: Standard test methods for determining the mechanical
536 properties of externally and internally threaded fasteners, washers, direct tension indicators, and
537 rivets.” ASTM International. West Conshohocken, PA.

538 ASTM (2017a). “ASTM A370-17: Standard test methods and definitions for mechanical testing
539 of steel products.” ASTM International. West Conshohocken, PA.

540 ASTM (2017b). “ASTM A6/A6M-17: Standard specification for general requirements for rolled
541 structural steel bars, plates, shapes, and sheet piling.” ASTM International. West Conshohocken,
542 PA.

543 ASTM (2017c). “ASTM E111-17: Standard test method for young’s modulus tangent modulus,
544 and chord modulus.” ASTM International. West Conshohocken, PA.

545 ASTM (2017d). “ASTM E132-17 (reapproved 2010): Standard test method for poisson’s ratio at
546 room temperature.” ASTM International. West Conshohocken, PA.

547 ASTM (2018). “ASTM F436/F436M-18a: Standard specification for hardened steel washers inch
548 and metric dimensions.” ASTM International. West Conshohocken, PA.

549 Gerbo, E. J., Thrall, A. P., Smith, B. J., and Zoli, T. P. (2016). “Full-field measurement of residual
550 strains in cold bent steel plates.” *Journal of Constructional Steel Research*, 127, 187–203.

551 Gerbo, E. J., Thrall, A. P., and Zoli, T. P. (2019a). “Adjustable bolted steel plate connection:
552 Measured behavior of bolts during field installation and numerical parametric investigation.”
553 *Journal of Structural Engineering* , In press.

554 Gerbo, E. J., Wang, Y., Tumbeva, M. D., Thrall, A. P., Smith, B. J., and Zoli, T. P. (2018). “Behavior
555 of an adjustable bolted steel plate connection during field installation.” *Journal of Structural
556 Engineering*, 144(3) , 04017223.

557 Gerbo, E. J., Wang, Y., Tumbeva, M. D., Thrall, A. P., Smith, B. J., and Zoli, T. P. (2019b). “Closure
558 to ‘Behavior of an Adjustable Bolted Steel Plate Connection during Field Installation’ by Evan
559 J. Gerbo, Yao Wang, Mirela D. Tumbeva, Ashley P. Thrall, Brian J. Smith, and Theodore P.
560 Zoli.” *Journal of Structural Engineering*, 145(3) , 07018015.

561 Kulak, G. L., Fisher, J. W., and Struik, J. H. A. (2001). *Guide to Design Criteria for Bolted and
562 Riveted Joints*. American Institute of Steel Construction, 2nd Edition, Chicago, I.L.

563 Research Council on Structural Connections (2014). “Specifications for Structural Joints Using
564 High-Strength Bolts.

565 SAE (2014). “SAE J429: Mechanical and material requirements for externally threaded fasteners.”
566 SAE International. Warrendale, PA.

567 **List of Tables**

568 1 Experimentally tested connection parameters. See Figure 1. 25

569 2 Measured material properties. E = elastic modulus, F_y = yield strength, F_u =
570 ultimate strength, ν = Poisson's ratio, Std. Dev. = standard deviation, COV =
571 coefficient of variation. 26

Scen.	γ (deg.)	α (deg.)	δ (deg.)	Other Parameters	e_b (mm)	Slip Load (kN)	e_h (mm)	Peak Load (kN)
1	0	0	0	Control	-1.59	29.0	0	154
2	0	0	0	Standard holes	-0.794	25.1	0	149
3a	10	12.5	2.5	Benchmark a	1.74	14.0	3.33	91.7
3b	10	12.5	2.5	Benchmark b	1.74	11.0	3.33	87.6
3c	10	12.5	2.5	Benchmark c	1.74	12.2	3.33	92.1
4	12.5	12.5	0		1.41	15.9	3.00	91.8
5	15	12.5	-2.5		1.37	16.6	2.95	95.9
6	10	12.5	2.5	Beveled washers	1.74	6.3	3.33	79.8
7	10	12.5	2.5	Increased tightening	1.74	-	3.33	-
8	10	12.5	2.5	Compression	1.74	12.6	3.33	35.8
9	0	2.5	2.5		-0.961	23.4	0.627	147
10	5	5	0		-0.404	26.4	1.18	114
11	5	7.5	2.5		0.376	23.0	1.96	90.7
12	5	2.5	-2.5		-1.01	24.4	0.578	150
13	10	10	0		0.797	20.2	2.38	87.6
14	10	7.5	-2.5		0.165	26.7	1.75	106
15	15	15	0		2.04	17.9	3.62	85.2
16	15	17.5	2.5		3.16	-	4.75	-

TABLE 1. Experimentally tested connection parameters. See Figure 1.

Component	Property	E (GPa)	F_y (Mpa)	F_u (Mpa)	ν
Plate	Mean	218	325	483	0.281
	Std. Dev.	7.01	2.54	1.04	0.00250
	COV %	3.21	0.784	0.215	0.215
Bolt	Mean	226	872	938	-
	Std. Dev.	8.41	23.4	10.9	-
	COV %	3.73	2.69	1.17	-

TABLE 2. Measured material properties. E = elastic modulus, F_y = yield strength, F_u = ultimate strength, ν = Poisson's ratio, Std. Dev. = standard deviation, COV = coefficient of variation.

572 **List of Figures**

573 1 Adjustable bolted steel plate connection including: (A) prefabrication via a press
574 brake, (B) isometric view of tightened connection, (C) elevation view of untight-
575 ened connection, (D) final tightened connection, (E) top flange bolt numbering, and
576 (F) bottom flange bolt numbering. Image (A) reprinted from Journal of Construc-
577 tional Steel Research, 127, EJ Gerbo, AP Thrall, BJ Smith, and TP Zoli, Full-field
578 Measurement of Residual Strains in Cold Bent Steel Plates, 187-203, 2016, with
579 permission from Elsevier. Images (B-F) adapted from Gerbo et al. (2019a) ©ASCE. 29

580 2 Experimental test setup: (A) Scenario 1 during bolt tightening, (B) Scenario 1 with
581 actuator applying load, (C) rendering of Scenario 1, (D) Scenario 3 during bolt
582 tightening, (E) Scenario 3 with actuator applying load, (F) rendering of Scenario 3,
583 (G) detailed view of Scenario 3, (H) instrumentation, (I) DIC measurement locations. 30

584 3 FE numerical model. 31

585 4 Measured actuator force, F , versus actuator displacement, Δ behavior for straight
586 and flush control tests and the adjustable bolted steel plate connection. Red indi-
587 cates flush ($\delta=0$), green indicates $+\delta$, and blue indicates $-\delta$ 32

588 5 Mechanisms for degradation in slip and bolt shear capacities: (A) δ -effect reducing
589 slip capacity, (B) interference-effect reducing slip capacity: friction from contact
590 due to plate bending, (C) interference-effect reducing slip capacity: catenary action
591 friction, (D) connection geometry leading to reduced bolt shear capacity. 33

592 6 Residual (i.e., after testing was completed) bolt deformations: (A) measured and
593 predicted full-field lateral, x displacements and (B) measured lateral location of
594 centerlines along the bolt axis, y 34

595 7 Measured slip along faying surfaces. 35

596 8 Effect of direction of loading: Measured actuator force, F , versus actuator dis-
597 placement, Δ behavior in tension and compression. 36

598	9	Effect of varying plate and member angles: Measured actuator force, F , versus	
599		actuator displacement, Δ behavior. Red indicates flush ($\delta=0$), green indicates $+\delta$,	
600		and blue indicates $-\delta$	37
601	10	Normalized measured slip loads, F_s compared to normalized analytical prediction	
602		of bolt deformation, e_b . Red indicates flush ($\delta=0$), green indicates $+\delta$, and blue	
603		indicates $-\delta$. Circles indicate predicted values considering mechanics-based re-	
604		ductions.	38
605	11	Normalized measured peaks loads, F_p compared to normalized analytical predic-	
606		tion of offset between the plate holes, e_h . Red indicates flush ($\delta=0$), green indicate	
607		$+\delta$, and blue indicates $-\delta$	39
608	12	Normalized measured DIC residual bolt shear deformations, s compared to nor-	
609		malized analytical prediction of offset between the plate holes, e_h for (A) top flange	
610		bolts and (B) bottom flange bolts. Red indicates flush ($\delta=0$), green indicates $+\delta$,	
611		and blue indicates $-\delta$	40
612	13	FE predictions of the axial force, B and moment, M in the bolt, along the axis of	
613		the bolt, y after field installation.	41

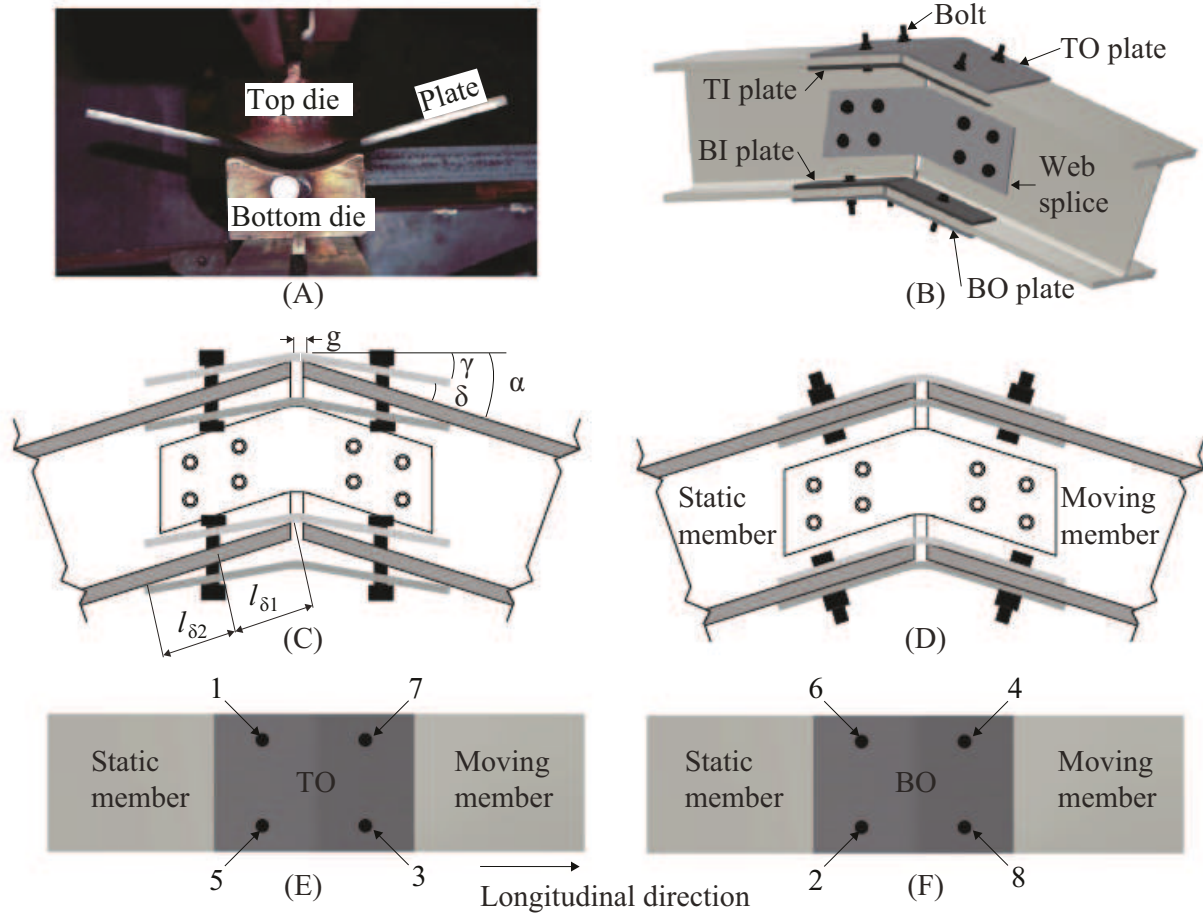


FIG. 1. Adjustable bolted steel plate connection including: (A) prefabrication via a press brake, (B) isometric view of tightened connection, (C) elevation view of untightened connection, (D) final tightened connection, (E) top flange bolt numbering, and (F) bottom flange bolt numbering. Image (A) reprinted from Journal of Constructional Steel Research, 127, EJ Gerbo, AP Thrall, BJ Smith, and TP Zoli, Full-field Measurement of Residual Strains in Cold Bent Steel Plates, 187-203, 2016, with permission from Elsevier. Images (B-F) adapted from Gerbo et al. (2019a) ©ASCE.

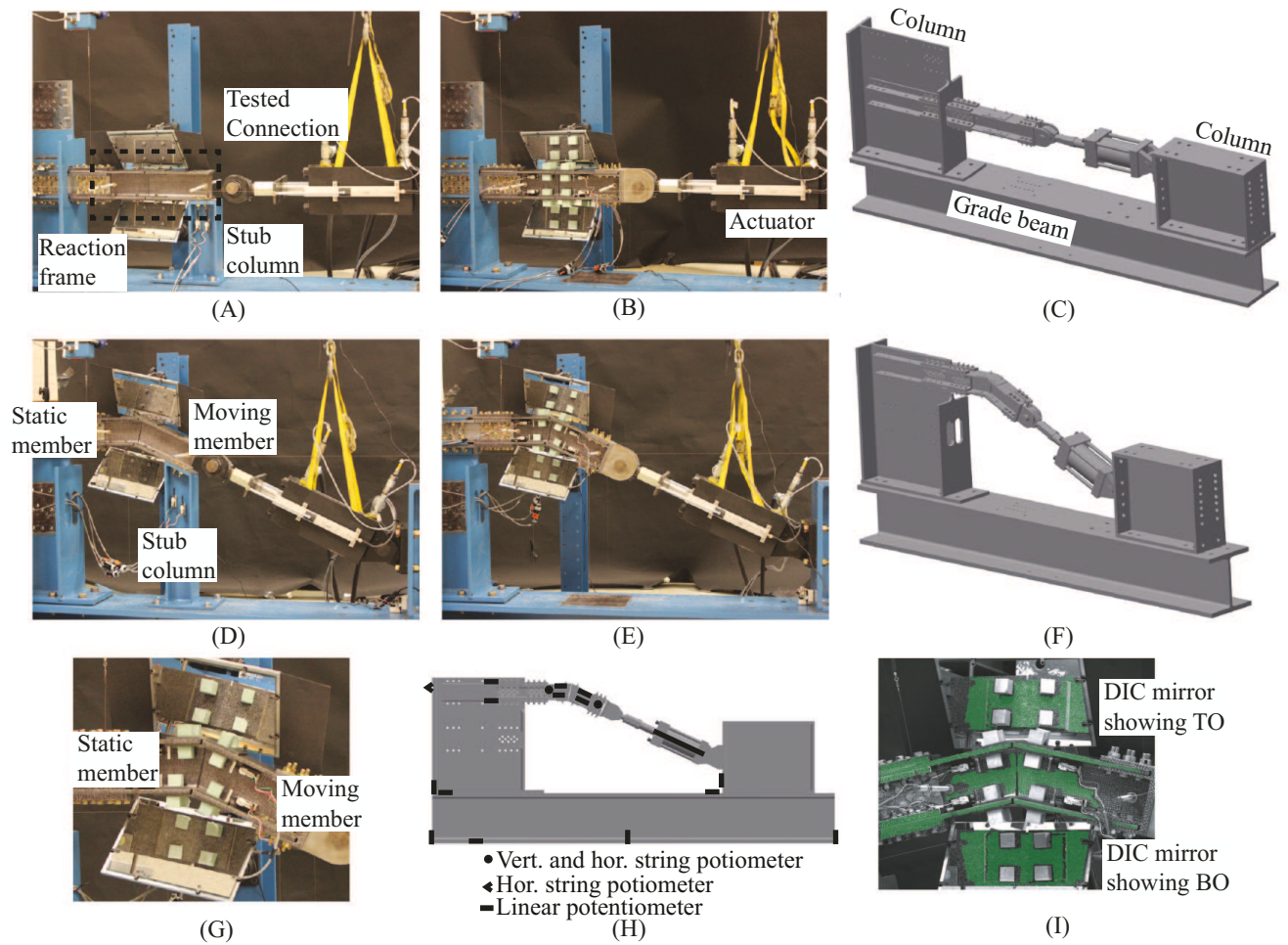


FIG. 2. Experimental test setup: (A) Scenario 1 during bolt tightening, (B) Scenario 1 with actuator applying load, (C) rendering of Scenario 1, (D) Scenario 3 during bolt tightening, (E) Scenario 3 with actuator applying load, (F) rendering of Scenario 3, (G) detailed view of Scenario 3, (H) instrumentation, (I) DIC measurement locations.

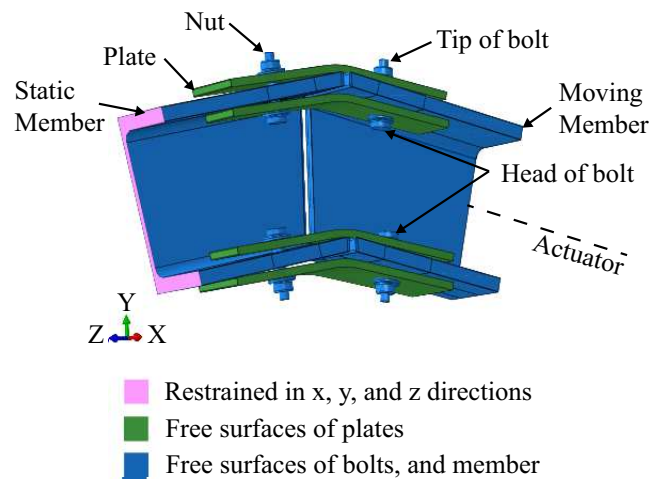


FIG. 3. FE numerical model.

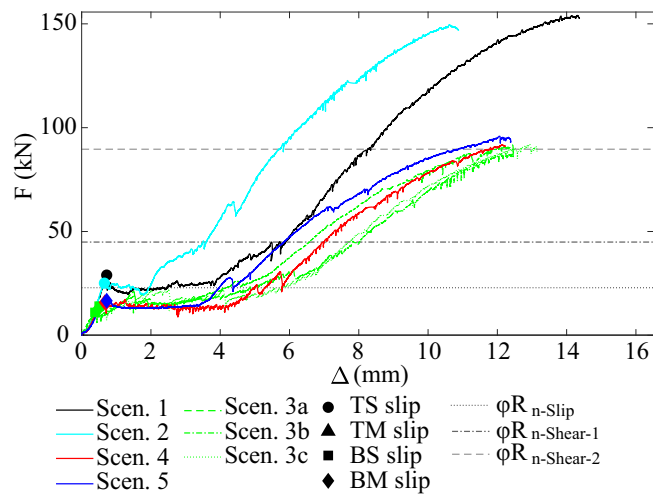


FIG. 4. Measured actuator force, F , versus actuator displacement, Δ behavior for straight and flush control tests and the adjustable bolted steel plate connection. Red indicates flush ($\delta=0$), green indicates $+\delta$, and blue indicates $-\delta$.

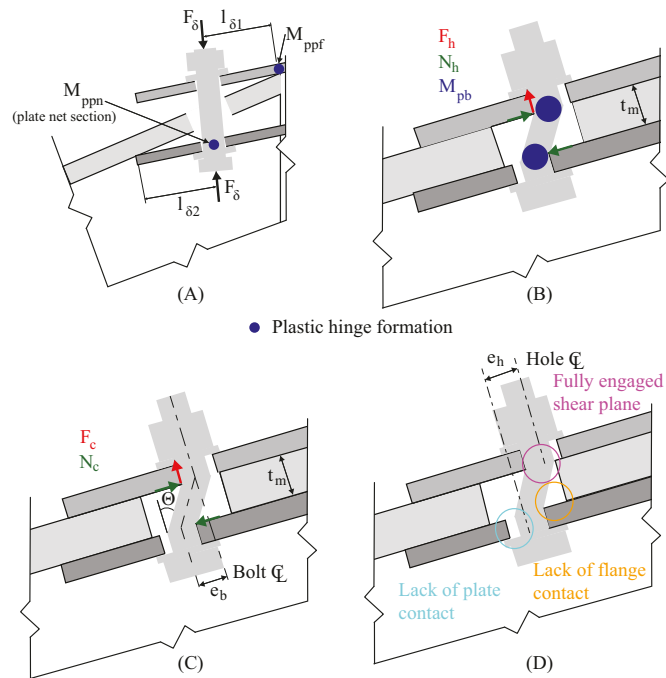


FIG. 5. Mechanisms for degradation in slip and bolt shear capacities: (A) δ -effect reducing slip capacity, (B) interference-effect reducing slip capacity: friction from contact due to plate bending, (C) interference-effect reducing slip capacity: catenary action friction, (D) connection geometry leading to reduced bolt shear capacity.

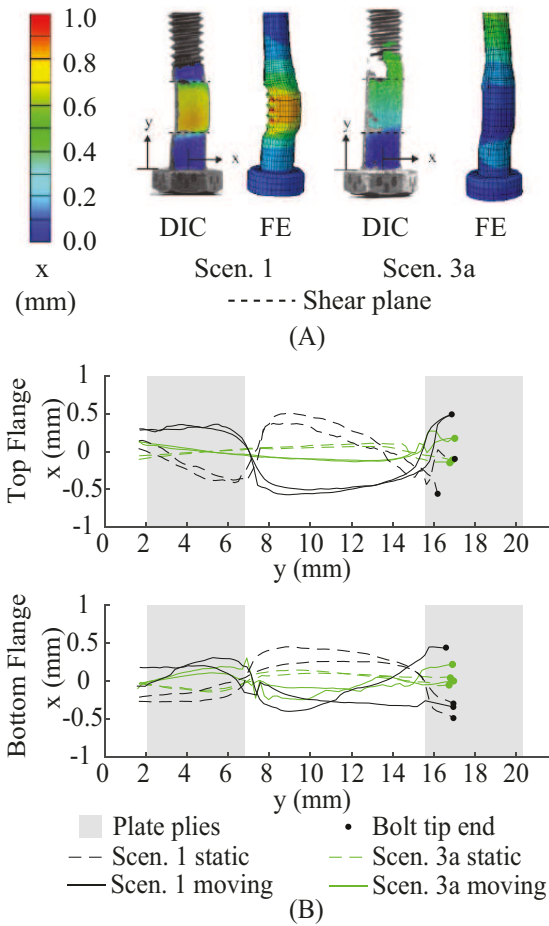


FIG. 6. Residual (i.e., after testing was completed) bolt deformations: (A) measured and predicted full-field lateral, x displacements and (B) measured lateral location of centerlines along the bolt axis, y .

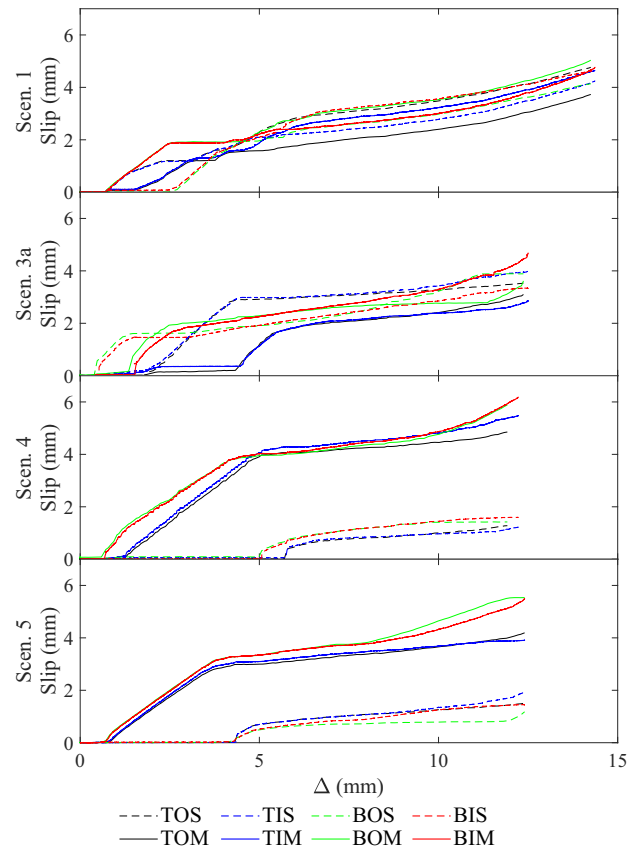


FIG. 7. Measured slip along faying surfaces.

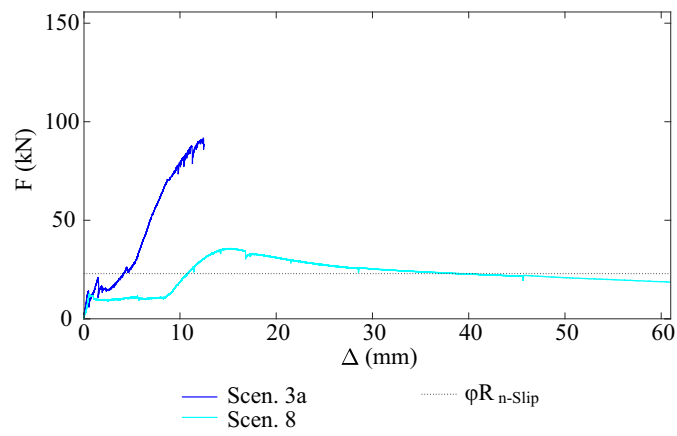


FIG. 8. Effect of direction of loading: Measured actuator force, F , versus actuator displacement, Δ behavior in tension and compression.

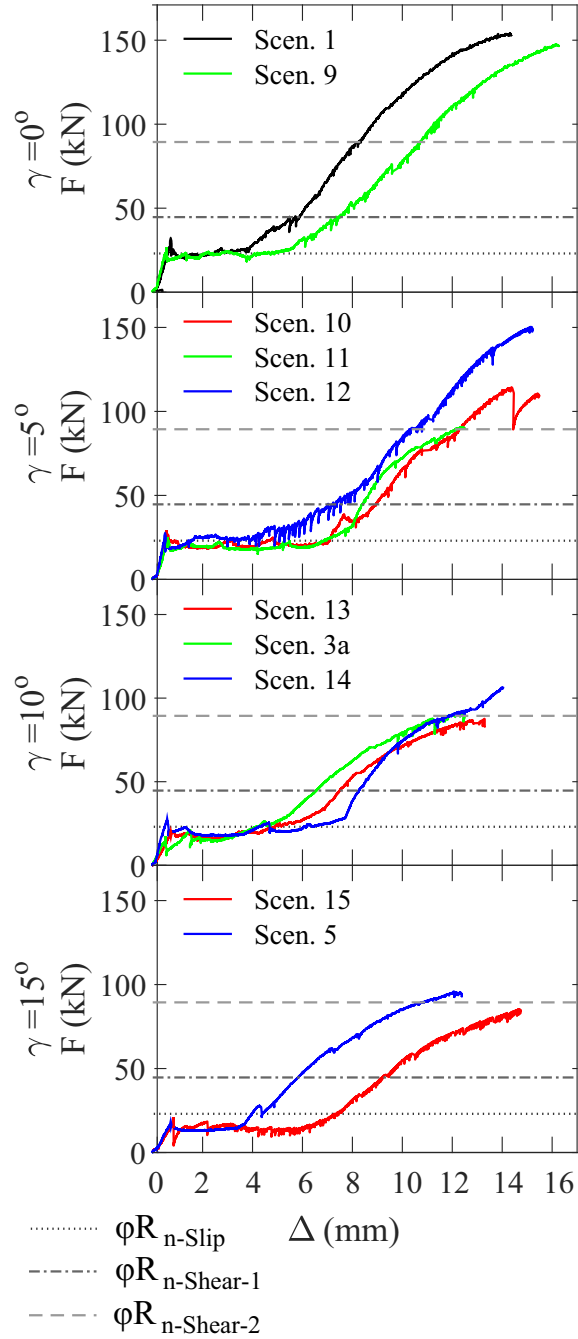


FIG. 9. Effect of varying plate and member angles: Measured actuator force, F , versus actuator displacement, Δ behavior. Red indicates flush ($\delta=0$), green indicates $+\delta$, and blue indicates $-\delta$.

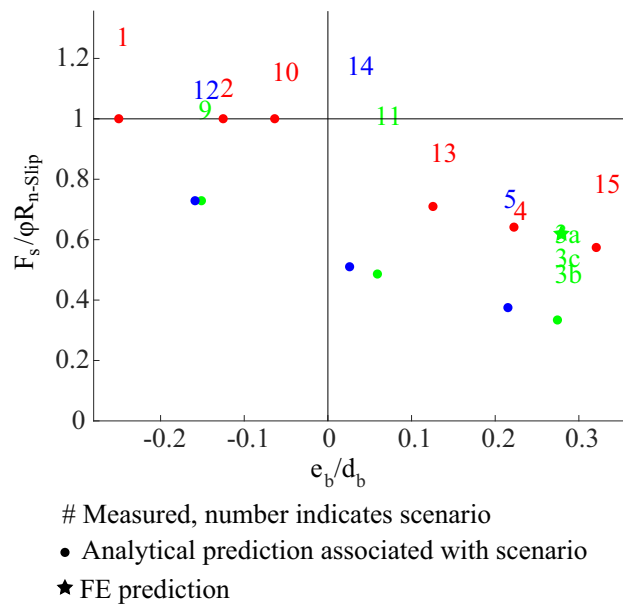


FIG. 10. Normalized measured slip loads, F_s compared to normalized analytical prediction of bolt deformation, e_b . Red indicates flush ($\delta=0$), green indicates $+\delta$, and blue indicates $-\delta$. Circles indicate predicted values considering mechanics-based reductions.

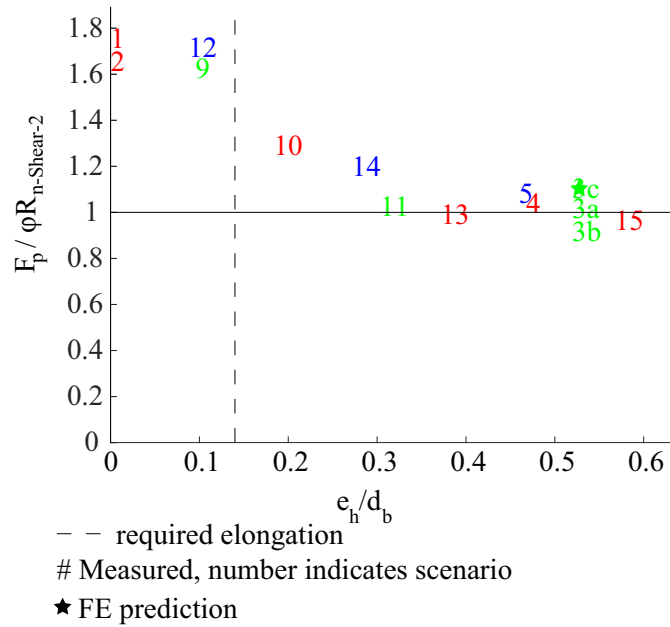


FIG. 11. Normalized measured peaks loads, F_p compared to normalized analytical prediction of offset between the plate holes, e_h . Red indicates flush ($\delta=0$), green indicate $+\delta$, and blue indicates $-\delta$.

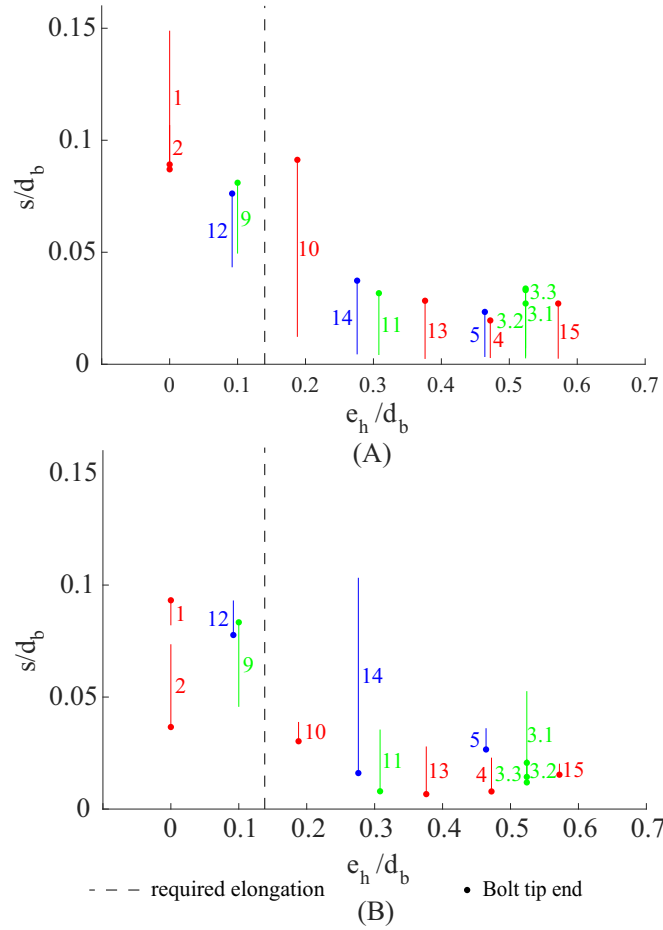


FIG. 12. Normalized measured DIC residual bolt shear deformations, s compared to normalized analytical prediction of offset between the plate holes, e_h for (A) top flange bolts and (B) bottom flange bolts. Red indicates flush ($\delta=0$), green indicates $+\delta$, and blue indicates $-\delta$.

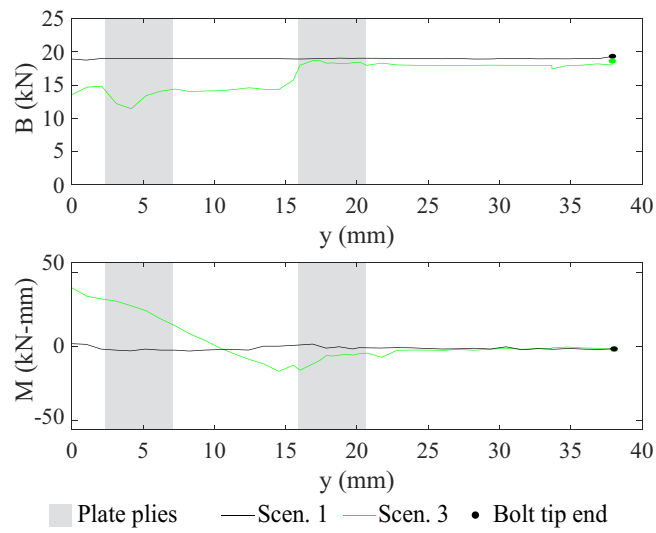


FIG. 13. FE predictions of the axial force, B and moment, M in the bolt, along the axis of the bolt, y after field installation.